Low-frequency radio study of MACS clusters at 610 and 235 MHz using the GMRT

Surajit Paul[1,2]⋆, Sameer Salunkhe[1], Abhirup Datta[3] and Huib T. Intema [4,5]

[1]*Department of Physics, Savitribai Phule Pune University, Pune 411007, India*
[2]*Inter University Centre for Astronomy and Astrophysics, Pune 411007, India*
[3]*Centre of Astronomy, Indian Institute of Technology Indore, Simrol, Khandwa Road, Indore 453552, India*
[4]*Leiden Observatory, Leiden University, Niels Bohrweg 2, 2333 CA, Leiden, The Netherlands*
[5]*International Centre for Radio Astronomy Research – Curtin University, GPO Box U1987, Perth, WA 6845, Australia*

arXiv:1903.06799v1 [astro-ph.HE] 15 Mar 2019

ABSTRACT

Studies have shown that mergers of massive galaxy clusters produce shocks and turbulence in the intra-cluster medium, the possible event responsible for creating observed radio relics, as well as the halo structures. Here we present GMRT dual-band (235 and 610 MHz) radio observations of four such merging cluster candidates from the MAssive Cluster Survey (MACS) catalogue. Clusters are chosen from their disturbed morphology in X-ray and elongated mass distribution in weak lensing study to ensure their merging state. Among the proposed four clusters, three of them are detected with diffuse radio emission. We report a flat spectrum ($\alpha \sim -1.15$), giant ($\sim$1.6 Mpc each) rare halo-relic system at low frequency radio waves from a previously known radio loud cluster MACSJ0014.3-3022 (commonly known as Abell 2744). Our observations have also revealed an ongoing second merger along with a close-by high-speed ($1769\pm^{148}_{359}$ km s^{-1}) merger-shock ($M = 2.02\pm^{17}_{41}$), thus providing a possible clue to the halo-relic co-existence. We also report the detection of very faint, diffuse radio relic like sources with size of about 0.4-0.5 Mpc in MACSJ0025.4-1222 (previously reported at 325 MHz) and MACSJ0152.5-2852 clusters. In both these clusters, proposed relics are found well inside the virial radius instead of their usual peripheral location, but, having no halos associated. These high-redshift objects (z=0.584 and 0.413) are possibly among the few known early and young merging galaxy clusters. We also report the non-detection of diffuse radio emission from the MACSJ1931-2635 cluster at the reported rms levels in our study.

Key words: (cosmology:) large-scale structure of Universe; observations – galaxies: clusters: general – radiation mechanisms: non-thermal; shock waves – radio continuum: general

1 INTRODUCTION

Clusters of galaxies are the largest ($\sim$ Megaparsec scale), gravitationally bound structures in the Universe. They are in general in thermal equilibrium and are prominent X-ray sources (Sarazin 1986). But, some of them are also detected at radio wavelengths (for review: Feretti et al. 2012; Giovannini et al., 1999), confirming the presence of cosmic-ray electrons and magnetic fields in the Intra-Cluster Medium (ICM). Radio sources connected to the ICM are mostly diffuse in nature, and have relatively steep spectra

($\alpha \lesssim -0.5$; van Weeren et al. 2009), suggesting ageing of the emitting particles (Feretti et al. 2012). This, in general, connects the emission to the Compton-synchrotron process where the highest energy electrons lose their energy more quickly during gyrations in magnetic fields present in the ICM (Bonafede et al. 2012; Nuza et al., 2012), known as ageing effect, that makes energy spectrum steeper. Steepening of the spectrum may also be related to the nature of the injection spectra due to the frequency dependence of particle acceleration mechanisms (Stroe, et al. 2014).

Diffuse radio sources are observed in a number of galaxy clusters (cf. review by Feretti et al. (2012)). These radio sources are not directly associated with the individual galax-

ies inside the cluster. Among them, the large-scale ($l \gtrsim 500$ kpc) diffuse radio sources are commonly divided into two broad classes, 'radio halos' and 'radio relics' (Kale et al. 2016; Feretti et al. 2012; Giovannini et al., 1999; Ensslin et al. 1998). Radio halos have smooth morphology, are extended with sizes $\gtrsim 1$ Mpc, steep spectrum, un-polarized and having low surface brightness ($\sim 0.1 - 1\ \mu$Jy arcsec^{-2} at 1.4 GHz; Giovannini et al. 2009; Feretti & Giovannini 2008), and are permeating the central volume of clusters almost co-spatial with the thermal X-ray emitting gas of the ICM (e.g. Abell 2219, Abell 2163 etc. Orrú et al. 2007; Feretti et al. 2001). Giant radio relics on the other hand, are mostly found at the periphery of the clusters, with sizes up to several Mpc, comparatively flatter spectrum and are highly polarized (p$\sim 10 - 50\%$ at 1.4 GHz; van Weeren et al. 2009). Though, the origin of thermal energy and X-rays in cluster of galaxies is quite explainable (Borgani & Guzzo 2001; Sarazin 1986), the exact origin of spectacular Mpc scale radio structures such as cluster peripheral relics, bow shock relics or giant radio halos etc. posses a tough challenge to the scientists.

Since, radio synchrotron emission from galaxy clusters is a transient phenomena (~ 0.5 Gyr) on cosmological time scales (Cassano et al. 2016), it is definitely connected to the dynamical states of the systems (Donnert et al. 2013; Paul 2012; Cassano et al. 2011; Rephaeli et al. 2008). Theoretically, in the large-scale structure formation framework, before attaining virialization, galaxy clusters pass through phases of continuous accretion and series of events of mergers of bigger and bigger galaxy groups (Sarazin 2002). Mergers are extremely energetic process and the energy released during mergers (ranging 10^{63-65} erg s^{-1}, depending on merging masses and impact angle) is dissipated in the ICM by thermalizing it through strong collision-less shocks (Sarazin 1986). These strong shocks with an efficient Fermi acceleration (of energetic charged particles), could generate strong MHD waves in the upstream and downstream regions of shocks and can strongly amplify the upstream magnetic field present in the ICM (Iapichino & Brüggen 2012; Bykov et al. 2008). This also transforms kinetic energy to turbulent energy by injecting volume-filling turbulence (Subramanian et al. 2006). Particle acceleration due to Diffusive Shock Acceleration (DSA) and magnetic field amplification due to shock compression is found to be highest at the shock fronts of high Mach number (Iapichino & Brüggen 2012; van Weeren et al. 2010). Therefore, shock fronts are expected to be detected well at radio frequencies, mainly in the peripheral regions (Brown et al. 2011; Paul et al. 2011). Turbulent re-acceleration supposed to dominate at the central part of the clusters, where the level of merger induced turbulent energy, availability of charged particles as well as fossil cosmic rays is very high, therefore produce the radio halo emission (Paul et al. 2018; Pinzke et al. 2017; Brunetti et al. 2001). The origin of both halos and relics would therefore be attributed to the mergers of galaxy clusters (Paul et al. 2018A; Nuza et al. 2017; Skillman et al. 2011; Paul et al. 2011; Cassano et al. 2010; Hoeft et al., 2007).

As, these structures are considered to be the direct consequence of major galaxy cluster mergers, they are mainly related to massive systems. In this study, we thus chose clusters from the MAssive Clusters Survey (MACS; Ebeling et al. 2010; Horesh et al. 2010; Ebeling et al. 2001) catalogue.

Table 1. Observation details

Cluster name	z	Obs. date	Obs. time
MACSJ0014.3-3022	0.308^a	13-AUG-2011	05:31 hour
		24-NOV-2006	04:42 hour†
MACSJ0025.4-1222	0.584^b	02-JUN-2011	03:43 hour
		& 05-JUL-2011	
		12-JAN-2014	03:40 hour†
MACSJ0152.5-2852	0.413^b	05-JUL-2011	04:50 hour
MACSJ1931.8-2635	0.352^a	03-JUN-2011	04:59 hour

Col. 1: cluster name

Col. 2: redshift (a:Ebeling et al. (2010), b: Horesh et al. (2010),

Col. 3: GMRT Observation date and Col. 4: On-source observation time

† This is an archival GMRT data at 325 MHz

The clusters are chosen here depending on their disturbed X-ray morphology and clumpy and elongated matter distribution as estimated from weak and strong lensing studies to ensure its merging phase. At the time of these observations, only one source i.e. MACSJ0014.3-3022, commonly known as Abell 2744, was known in radio waves. A large halo and a relic was first reported at VLA 1.4 GHz (Govoni et al. 2001a,b) Later, in MACSJ0025.4-1222 a double relic has also been discovered at GMRT 325 MHz by Riseley et al. (2017). We decide to perform a low-frequency radio spectral and morphological study at GMRT 235 and 610 MHz as, in general, diffuse radio emission from clusters are steep spectrum ($\alpha \leq -1.0$) and expected to be better detected at low-frequencies.

We introduce our work in Section 1. Selection of clusters of galaxies, observation details and data analysis are described in Section 2. In the result Section 3, we report our findings from each observed objects. Thereafter, we discus our findings in Section 4 and finally, conclude the paper in Section 5. Cosmology used in this study is as follows: $H_0 = 70.2 km\ s^{-1}\ Mpc^{-1}$, $\Omega_m = 0.274$ and $\Omega_\Lambda = 0.726$.

2 OBJECT SELECTION, GMRT OBSERVATIONS AND DATA ANALYSIS

2.1 Selected objects

The principal goal of this work is to obtain the dynamical features of a few chosen galaxy clusters through their radio morphology and spectral properties. As discussed in Section 1, several studies attribute the origin of radio sources to the mergers of massive systems. Thus, we obtain deep GMRT radio maps of diffuse emissions from four massive galaxy clusters (see Table 1) chosen from the MACS catalogue. This cluster survey was designed to find the population of strongly evolving clusters, with the most X-ray luminous systems using a specific X-ray selection function described in (Ebeling et al. 2001). From the MACS catalogues (up to 2010; Ebeling et al. 2007, 2010) we have selected clusters that are showing clear merging activity in X-ray/temperature maps and also from mass distributions obtained from weak lensing studies (See Zitrin et al. 2011 and Table 1).

In radio waves, cluster Abell 2744 had previously been studied at high frequency with wideband VLA 1-4 GHz and 1.4 GHz by (Pearce et al. 2017; Govoni et al. 2001a,b). In

Table 2. Data analysis details

Cluster name	Frequency (MHz)	Robust	UV taper (Kilo-lambda)
MACSJ0014.3-3022	235 & 610	-1.0	10
	325*	-1.0	0
MACSJ0025.4-1222	235 & 610	0.5	0
	325†	0.5	0
MACSJ0152.5-2852	235 & 610	-1.0	10
MACSJ1931.8-2635	235 & 610	-1.0&0.5	10&0

Col. 1: cluster name

Col. 2: Observation central frequencies

Col. 3: Robust parameter used for imaging

Col. 4: UV taper used in Kilo-lambda.

∗ Re-analysed 325 MHz data reported in Venturi et al. (2013)

† Re-analysed 325 MHz data reported in Riseley et al. (2017)

low frequency, except 325 MHz at VLA & GMRT (Orrú et al. 2007; Venturi et al. 2013), no deeper radio study has been reported yet (except our partly reported proceedings Paul et al. 2014). Though George et al. (2017) has reported 88-200 MHz (GLEAM) and 150 MHz (TGSS) images both are from survey data having very poor resolution and sensitivity to study the substructures and spectral properties very accurately. MACSJ0025.4-1222 has also been studied previously but only at GMRT 325 MHz (Riseley et al. 2017).

2.2 GMRT observations

Observations were done with Giant Metre-wave Radio Telescope (GMRT) array using 235 & 610 MHz dual-band during June - August 2011 (Project Code : 20_062). Observation details are provided in Table 1. In this mode of observation at GMRT, each frequency is observed simultaneously with only one of the polarizations. Although, the observations were recorded over 32 MHz band for both the frequencies, for 235 MHz observation, only a part of that bandwidth is available due to use of a bandpass filter. The dual-frequency observations were chosen to compute the spectral properties of these sources. The GMRT is very much suitable for observing these objects, as it has both adequate short baselines (14 antenna's within 1 square km with shortest at 100 m) and long baselines (with the longest baseline of 26 km). Good coverage of short spacings enabled us to map the diffuse emission and long spacings give the high resolution to resolve the important substructures present in these objects. Each of the proposed sources was observed with almost 4-5 hours of on-source time. Special care was taken to preserve maximum possible short baselines during the observations to we properly image most of the diffuse radio emissions from these sources. Along with our dual frequency GMRT data, we have also analysed GMRT archival data of Abell 2744 and MACSJ0025.4-1222, both at 325 MHz for this study.

2.3 Data analysis

We split the LL and RR correlations to obtain two data sets at two different frequencies i.e., 235 MHz and 610 MHz from our GMRT dual frequency mode observations. For 325 MHz, combined RR-LL data was taken. Further, data analysis and imaging were done with the code 'SPAM' (for de-

tails see Intema et al. 2017) using the parameters given in Table 2. Here we mention those parameters with which we have obtained the best images in terms of our requirements for this study. 'SPAM' is a powerful data analysis and imaging pipeline that takes care of direction dependent variations (i.e. due to antenna beam pattern and due to ionosphere) in visibility amplitude and phase, across the field of view. The initial flux and bandpass calibrations were done using the source 3C48 for the target sources Abell 2744, MACSJ0152-2852 and MACSJ0025-1222 and the source 3C286 for target source MACSJ1931-2635.

High resolution images were first made with robust −1.0 to map the point and bright sources and to check for any indication of diffuse radio emission in the imaged fields. Further, to catch the diffuse emission better, UV taper at 10 Kilo lambda was used for both the frequencies. For some images, different robust parameters (see Table 2) were used to obtain better diffuse emission or rms values as per the requirements of our study. As the observation of the object MACSJ0025-1222 was spread over two days, two data sets were combined to make a single data set for imaging. 325 MHz image of Abell 2744 was made with robust −1, and beam was convoluted to $35'' \times 35''$ size to match the resolution of Venturi et al. (2013). Other archival data of MACSJ0025.4-1222 at GMRT 325 MHz was analysed with robust 0.5, same as the parameters used for 235 and 610 MHz data for the same object. Data from only one session from Riseley et al. (2017) was taken to keep the total observation time similar to ours (see Table 1). All the post-pipeline analysis were done and measurements were taken using the Common Astronomy Software Applications (CASA) package (McMullin et al. 2007).

2.4 Estimation of upper limits for the radio halos

We estimate the radio halo upper limits for the clusters in which no radio halo is detected, but found other diffuse radio emissions. In recent years, various researchers have formulated different strategies for computing upper limits for radio halos in galaxy clusters (Venturi et al. 2008; Bonafede et al. 2017; Johnston-Hollitt & Pratley 2017). Usually, as a first step, a fake radio halo is injected either as an optically thin sphere (Venturi et al. 2008), elliptical (Johnston-Hollitt & Pratley 2017) or an exponentially decreasing radio profile (Bonafede et al. 2017) with the help of specific tasks in AIPS, MIRIAD or CASA. Each of the tasks modifies the UV data set depending on the injected artificial source parameters. An image is then made from this modified UV data, and an upper limit is estimated with a criteria of bare detection of this injected halo in the final image.

In this paper, we grossly follow the method used in Bonafede et al. (2017) with slight modification. Since average brightness profile for observed, nearly ideal radio halos found to fit well with the exponential curve (Murgia et al. 2009), we have injected the exponential fake radio halo profiles as suggested by Bonafede et al. (2017) and thereafter computed the upper limit. The basic algorithm used by us to estimate the halo upper limit is described below.

(i) First, we calculate the expected radio power for inject-

ing the mock radio halo from the correlation of $P_{1.4GHz}$ and M_{500} given in Cassano et al. 2013 i.e.,

$$\log\left(\frac{P_{1.4}}{10^{24.5}\,Watt\,Hz^{-1}}\right) = B\,\log\left(\frac{M_{500}}{10^{14.9}\,M_\odot}\right) + A \qquad (1)$$

where $A = 0.125 \pm 0.076$ and $B = 3.77 \pm 0.57$ are BCES-bisector fitting parameters for 'Radio Halo' only data.

(ii) This radio power is used to calculate the expected size of the radio halo from direct scaling relation of 1.4 GHz radio power $P_{1.4GHz}$ and R_H i.e. radii of radio halos (Cassano et al. 2007) and is given by

$$\log\left(\frac{P_{1.4}}{5\times10^{24}\,h_{70}^{-2}\,W\,Hz^{-1}}\right) = 4.18 \pm 0.68 \log\left(\frac{R_H}{500h_{70}^{-1}\,kpc}\right)$$
$$-0.26 \pm 0.07 \qquad (2)$$

The flux density corresponding to the expected power is $S_{R_H}^{mock,inj}$ i.e. injected flux.

(iii) After calibrating our 610 MHz UV data using SPAM, we take the data into AIPS. Thereafter, an exponential halo is injected into the uv-plane with expected radio power within the expected radius using the task UVMOD. Though we calculate the expected radio power at 1.4 GHz, corresponding value at 610 MHz has been calculated taking the spectral index of $\alpha = -1.3$ between 1.4 GHz and 610 MHz and the size of the halo is kept same, assuming no significant variation due to change in frequency. Further, we take back this modified UV data with this mock halo to SPAM and image it. This is done to keep the method of imaging consistent throughout the study.

(iv) In this final image with mock halo, a halo is said to be detected if $D_{2\sigma}^{mock,meas} \geq R_H$; where $D_{2\sigma}^{mock,meas}$ is the size the halo measured above 2σ and the corresponding flux is said to be $S_{2\sigma}^{mock,meas}$.

(v) Now, if $D_{2\sigma}^{mock,meas} > R_H$ and $S_{2\sigma}^{mock,meas} \gg 30\%S_{R_H}^{mock,inj}$, then the value of flux to inject radio halo is decreased, and if $D_{2\sigma}^{mock,meas} < R_H$ then the value of flux to inject radio halo is increased.

(vi) We repeat steps 2 to 5, until we get the halo for which recovered flux is at least 30% of the injected and the total size of the halo is around the expected radius of the halo i.e. $D_{2\sigma}^{mock,meas} \gtrsim R_H$.

2.5 Estimation of flux error and spectral index

We compute the flux densities (S) of observed radio sources within 3σ (σ is noise rms of the image) and flux density errors (σ_S) using the usual relation i.e.,

$$\sigma_S = \sqrt{0.1S^2 + N\sigma^2} \qquad (3)$$

Where N is the number of beams covered by the total diffuse emission and $0.1S$ (i.e. 10% of S) is assumed to be the possible error due to calibration uncertainties.

The spectral index map has been created after regridding the two images of different frequencies using the

IMREGRID task of CASA. The images used for making spectral index maps are made with uniform weights. Since beam sizes are not usually the same, we convolute the beam of 610 MHz image with the beam of 235 MHz using IMSMOOTH task. The images were then masked at 3σ contour of 235 MHz image. Finally, we compute the spectral index using IMMATH with the relation

$$\alpha = \frac{\log S_{\nu_2} S_{\nu_1}}{\log \nu_2 \nu_1} \qquad (4)$$

Where $S_{\nu_\#}$ and $\nu_\#$ (with $\nu_1 > \nu_2$) are the values of flux density and the frequency of observation respectively.

Further, we calculate the spectral index error with IM-MATH task using the relation given below (Kim & Trippe 2014)

$$\alpha_{err}\alpha_{\nu_2,\nu_1} = \frac{1}{\log\nu_2\nu_1} \times \left[\frac{\sigma_{\nu_1}^2}{I_{\nu_1}^2} + \frac{\sigma_{\nu_2}^2}{I_{\nu_2}^2}\right]^{\frac{1}{2}} \qquad (5)$$

With I as the total intensity at respective frequencies at each of the pixels.

3   RESULTS

In Table 3, we summarise our findings. We mention the detected radio structures in the chosen clusters at different frequencies and respective rms values with the beam sizes. We also report the angular sizes of the observed diffuse radio structures, corresponding flux densities and luminosities. For halos, the sizes are reported as North-South (NS) and East-West (EW) but relic sizes are taken as Largest Linear Size (LLS) and the average width as given in the Table 3. We also include here the values of various parameters measured from the re-analysed GMRT 325 MHz archival data of two clusters, namely Abell 2744 and MACSJ0025.4-1222.

The results from the individual clusters are presented below.

3.1   MACSJ0014.3-3022 or Abell 2744

The Cluster Abell 2744 is a moderately distant cluster at redshift z=0.308. This is a very hot and massive cluster with average temperature of 8.53±0.37 keV (Mantz et al. 2010). Radius and mass are estimated to be $r_{500} = 1.65\pm0.07$ Mpc and 17.6±2.3 $10^{14}\,M_\odot$ respectively (Ebeling et al. 2010). Importantly, the authors found no cooling flow in the cluster but, presence of substructures in X-rays indicate an ongoing merging process. Interestingly, it is also one of the HST frontier fields (Mahler et al. 2018).

This object is known for hosting a radio halo, as well as relics, as reported in various studies (George et al. 2017; Pearce et al. 2017; Venturi et al. 2013; Orrú et al. 2007; Govoni et al. 2001b). We detect both the relics and an extremely large halo (Both Panels in Fig 1) at GMRT low-frequency dual band observation (610 and 235 MHz). A high resolution 235 MHz map with Chandra X-ray contours (Fig. 2) reveals that the more prominent radio halo emission is associated with the substructure that has crossed the core of the system, and moving towards the South-East (SE) direction of the map (in RA-DEC plane). Chandra X-ray contours

**Table 3.** Radio properties of the sources

Cluster name	Source/ Emission	Frequency (MHz)	Beam size	rms (μJy beam^{-1})	Size	S (mJy)	Luminosity (10^{24} W Hz^{-1})
Abell 2744	Halo	610	$20.62'' \times 15.83''$ PA $4.27°$	100	$300'' \times 275''$	103.25 ± 10.40	31.84 ± 3.21
	Relic A				$325'' \times 105''$	46.78 ± 4.74	14.43 ± 1.46
	Relic B				$190'' \times 35''$	4.28 ± 0.54	1.32 ± 0.17
	† ⌠Halo	325	$35.0'' \times 35.0''$ PA $0.0°$	450	$370'' \times 350''$	307.72 ± 30.98	89.97 ± 9.03
	⌡Relic A				$400'' \times 155''$	118.69 ± 12.11	35.59 ± 3.60
	⌡Relic B				$162'' \times 39''$	8.62 ± 1.33	2.15 ± 0.30
	Halo	235	$25.55'' \times 17.42''$ PA $-2.15°$	360	$275'' \times 270''$	302.26 ± 30.49	93.22 ± 9.40
	Relic A				$325'' \times 100''$	123.05 ± 12.61	37.94 ± 3.89
	Relic B				$215'' \times 45''$	12.63 ± 1.78	3.90 ± 0.55
MACSJ0025	Relic	610	$6.34'' \times 5.84''$ PA $34.66°$	90	$53'' \times 9''$	1.98 ± 0.30	2.81 ± 0.42
	Relic	325	$13.52'' \times 10.91''$ PA $-65.41°$	200	$68'' \times 26''$	5.08 ± 0.75	7.20 ± 1.06
	?	235	$15.53'' \times 12.17''$ PA $0.01°$	700	–	–	–
MACSJ0152	Relic ?	610	$18.89'' \times 15.91''$ PA $-2.43°$	70	–	–	–
	Relic ?	235	$22.28'' \times 16.39''$ PA $-5.96°$	500	$65'' \times 30''$	9.24 ± 1.30	5.68 ± 0.80
MACSJ1931	Galaxy	610	$7.55'' \times 5.22''$ PA $-1.06°$	80	–	–	–
	Galaxy	235	$17.37'' \times 11.93''$ PA $4.09°$	1200	–	–	–

Col. 1: cluster name **Col. 2:** Possible type of source or emission structures **Col. 3:** Frequency of observation **Col. 4:** Image beam size in arc second.
Col. 5: Image rms (σ) in μJy beam^{-1} **Col. 6:** Size of the structures **Col. 7:** Flux density in mJy **Col. 7:** Luminosity of the sources in 10^{24} W Hz^{-1}.
† Size, flux density and Luminosities are calculated within 1 mJy contour to compare with Venturi et al. (2013) values.
(? means-proposed or doubtful.)
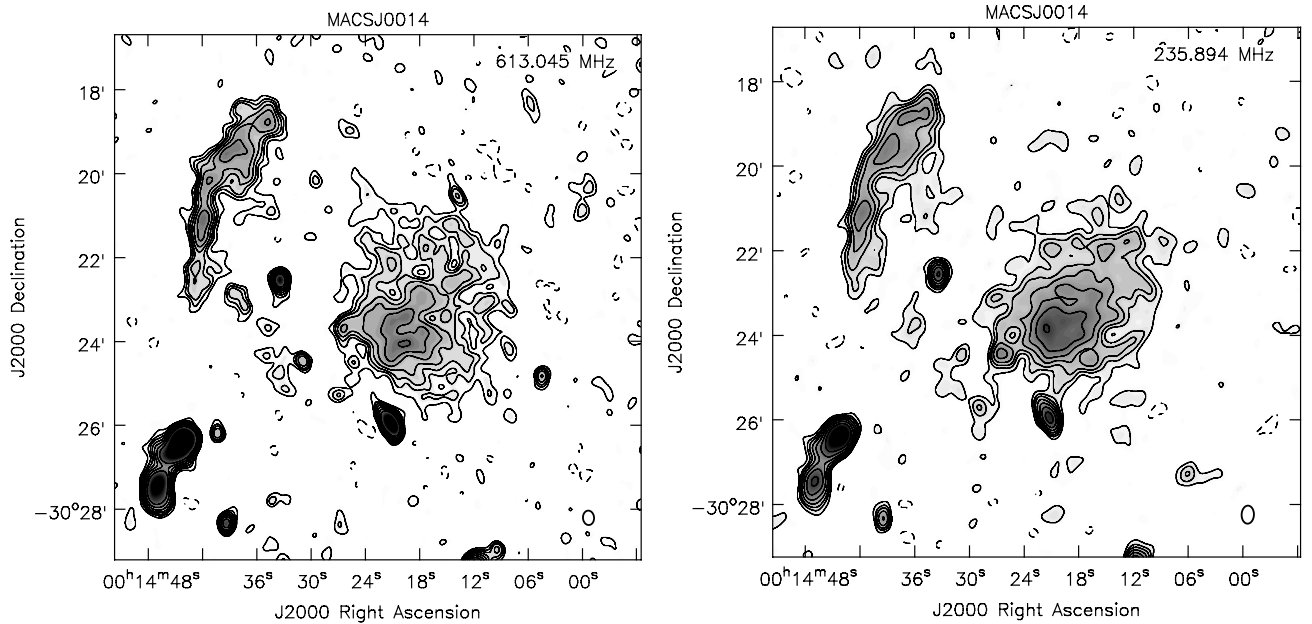
Figure 1. Panel 1: 610 MHz GMRT radio continuum map of MACSJ0014.3-3022 or Abell 2744 plotted as grey colour and black contours are at the level of 3σ (where rms i.e. $\sigma = 100\mu$Jy beam^{-1}) and rest of the 6 contours are in multiplication of $\sqrt{2}$ of first contour. A negative contour at -3σ has been plotted as dashed line. **Panel 2:** Similar image and contours of the same cluster at GMRT 235 MHz. Only this time the $\sigma = 360\mu$Jy beam^{-1}.

clearly shows two substructures, both are reported to be associated with bow shocks placed in the SE direction from each of these sub-clumps Kempner & David (2004). In this high resolution radio map (Fig. 2), only brightest and sharp relic edge has been observed. Plenty of point sources that can be seen in X-rays are mostly found to be not associated

with the radio halo or relic emissions confirming its diffuse nature.
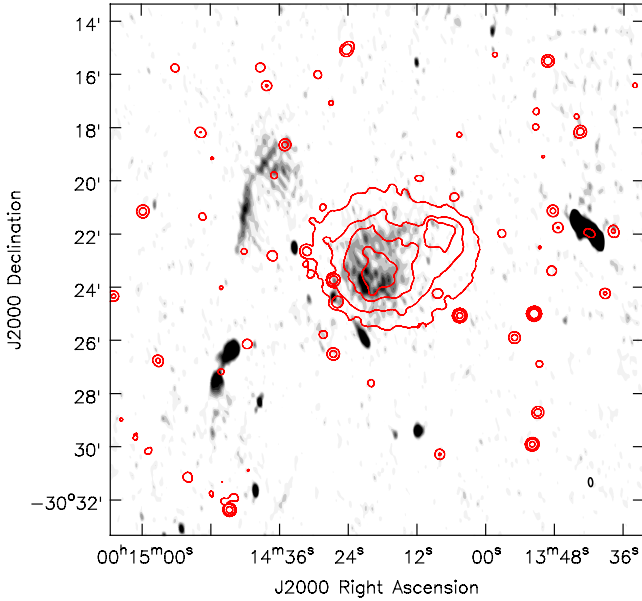
Figure 2. GMRT 235 MHz high resolution radio map of Abell 2744 in gray colour. Rms of the image is 280 μJy beam^{-1} with a beam of $19.94'' \times 9.56''$ PA=4.8°. Chandra X-ray (0.5-7.0 keV, Gaussian smoothed) contrours are over-plotted in red colour with contours at 4,8,16 and 32 times 10^{-8} photons s^{-1} cm^{-2} pixel^{-1}.

Figure 3. Contours at 610 (black) and 235 MHz (red) are plotted together for cluster Abell 2744. Contours are same as in Figure 1. Blue dashed circle encloses the radio halo, black dashed region shows the relic B and almost concentric circular arc with dashed black line indicates the outer edge of the relic A i.e. shock front.

3.1.1   Radio halo

Radio halo in this cluster is a copybook halo, truly representing its class having almost circular shape (see Fig. 3, blue dashed circle), possibly spherical in 3D. But, the peak emission is located towards the SE corner of the halo, indicating movement of this bigger merging sub-clump to this direction. The halo is almost similar in shape and morphology in both the frequencies, as it can be noticed in the overlapped map in Figure 3. But, the sub-structures at different frequencies are appearing at different positions. At 610 MHz, a split in the halo centre can also be found (see Fig. 1, Panel 1). The halo is also observed to be inflated a bit towards the relic.

At 610 MHz, the image has 1σ i.e. rms value of 100 μJy beam^{-1} with a beam of $20.62'' \times 15.83''$ and PA 4.27°. Similarly at 235 MHz, the rms is 360 μJy beam^{-1} with a beam of $25.55'' \times 17.42''$ and PA -2.15°. The lowest contour is plotted with 3σ and further 6 contours are at intervals of square root of 2 of the first contour (see Fig. 1). A negative contour has also been shown at -3σ. This radio halo roughly has a regular morphology with a projected angular size (LLS i.e. Largest Linear Size) of about 6′ ($\sim$ 1.6 Mpc) as found at about 3σ detection limit at both frequencies (See Table 3 for detailed observed parameters). Our re-analysed GMRT 325 MHz map measures a larger LLS of 1.85 Mpc (image not shown), comparable to the reported $\sim$ 1.9 Mpc Venturi et al. (2013), both measured within the contour level of 1 mJy/beam. The flux densities at 235 and 610 MHz respectively are given by 302.26 ± 30.49 and 103.25 ± 10.40 mJy, where error has been computed using the Eq. 3. We detect more structures and larger extension of the halo at GMRT 325 MHz. The reported flux density of the halo is also higher at 323 ± 26 mJy (Venturi et al. 2013). Whereas, our measured value is 308 ± 31 mJy (Detail in Table 3).
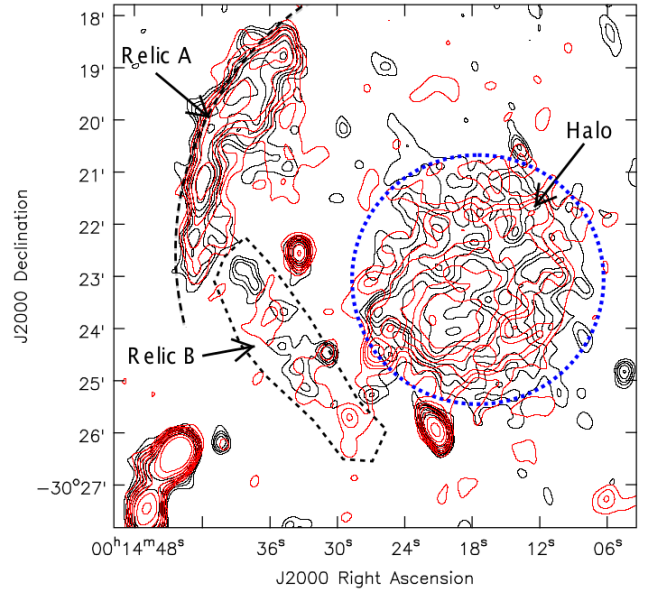
3.1.2   Radio relic

The most prominent radio relic (Relic A as shown in Fig. 3) in this cluster is a peripheral single, bow-shaped relic with concave side facing towards the cluster centre. It follows well the curvature of the radio halo structure, as shown in Fig. 3 with almost concentric circles (dashed Black and Blue). As, we have discussed above, the motion of the merging clumps is towards the SE corner. But, the relic is towards North-East (NE) corner i.e., perpendicular to the possible merging axis. The relic A has several sub-structure emissions and is not sharp edged like the CIZA J2242.8+5301 cluster (Stroe et al. 2013). Interestingly, the peripheral curved relic in this cluster has almost the same length as the halo 5.5′ ($\sim$ 1.5 Mpc) at 235 and 610 MHz and 1.82 Mpc in 325 MHz and a large average width of about 500 kpc in all the reported frequencies (see Table 3). The relic is placed at about 1.7 Mpc (365″) away from the cluster centre i.e., at about r_{500} radius of the said cluster.

A second relic, Relic B, as shown in the image (Fig. 1, both panel) can be seen just in front of the bigger merging group that has crossed the centre and moving towards the SE corner. This relic is faint and broken into parts (as seen above 3σ level). Broken parts in different frequencies do not totally co-inside, rather complement each other to make a full shock front. The full shock thus can be recovered by over-plotting emission from these two different frequencies, as shown in Figure 3, indicated as Relic B within the black dashed area. Pearce et al. (2017) has also reported this relic at high frequency, wide band VLA 1-4 GHz map and Venturi et al. (2013) has mentioned it as a radio bridge between halo and the Relic A as found in their GMRT 325 MHz low resolution map.

Relic A is a bright radio source with flux densities

Table 4. Total spectral index of the detected structures

(235-610 MHz)			
Cluster name	Halo/relic	Spectral index	Error
Abell 2744	Halo	-1.17	± 0.33
	Relic A	-1.14	± 0.36
	Relic B	-1.65	± 0.62
(235, 325 & 610 MHz)			
Abell 2744	Halo	-1.21	± 0.20
	Relic A	-1.09	± 0.20
	Relic B	-1.34	± 0.16

Col. 1: Cluster name **Col. 2:** Type of radio structures **Col. 3:** Average spectral index of the total structures **Col. 4:** Error in spectral index.

46.78 ± 4.74, 118.69 ± 12.11 and 123.05 ± 12.61 mJy and integrated power of $1.44 \pm 0.15 \times 10^{25}$, $3.56 \pm 0.36 \times 10^{25}$ and $3.79 \pm 0.39 \times 10^{25}$ W Hz^{-1} at 610, 325 and 235 MHz respectively. For the same relic, Venturi et al. (2013) has reported a total flux density of 122 ± 10 mJy within 1 mJy contour at 325 MHz. Since, the Relic B is in discrete parts at 3σ level in each frequency, we have measured the flux from a polygonal common area at these frequencies. The respective flux densities are 5.83 ± 0.98, 12.08 ± 2.09 and 24.84 ± 3.66 mJy and corresponding total radio power is $1.80 \pm 0.30 \times 10^{24}$, $3.72 \pm 0.64 \times 10^{24}$ and $7.65 \pm 1.13 \times 10^{24}$ W Hz^{-1} i.e., having values almost an order lower in magnitude compared to the Relic A.

3.1.3 Spectral index

Spectral index map of 610 and 235 MHz emission has been produced using the method described in Section 2.5 and shown in Figure 4, Panel 1. It can be noticed that the radio halo has a flat spectrum with average value of about $\alpha_{halo\,235}^{610} = -1.17 \pm 0.33$. Except few small patches of extreme flat spectral index ($<< -1.0$), mostly the spectrum is uniform (~ 1.1) throughout the halo. The corresponding error map computed using Eq. 5 has been shown in Figure 4, Panel 2. Further, combined spectral index has been computed using 235, 325 and 610 MHz fluxes considering a common area of the halo and relic. Only a slight change in the spectral index of $\alpha_{halo} 235, 325, 610 = -1.21 \pm 0.20$ is observed. Computed spectral index and error for various components of the Abell 2744 cluster have been tabulated in Table 4. Average or integrated spectral index of the relic A is $\alpha_{relA_{int}\,235}^{610} = -1.14 \pm 0.36$. On the outer age of the relic is shown to have a very flat spectrum of $\alpha_{relA-E\,235}^{610} = -0.69 \pm 0.21$. This steepens gradually towards the inner side of the relic to about $\alpha_{relA-O\,235}^{610} = -1.29$. Therefore, it seems, it follows the usual injection model reasonably i.e., $\alpha_{inj\,235}^{610} = \alpha_{int\,235}^{610} - 0.5 = 0.64 \sim \alpha_{relA-E\,235}^{610}$. Injection spectrum of relic A i.e., $\alpha_{relA-E\,235}^{610} = -0.69 \pm 0.21$ corresponds to the highest Mach number of about $M = 3.40$ to the lowest of $M = 2.45$ at the injection. Where Mach number has been computed as

$$M^2 = \frac{2\alpha + 3}{2\alpha - 1} \qquad (6)$$

considering DSA mechanism (Blandford et al. 1987; Colafrancesco et al. 2017). The average Mach number of this shock is $M = 2.03$ (as average $\alpha_{relA_{int}\,235}^{610} = -1.14$), which corroborates to the study of (Pearce et al. 2017). However, X-ray detected thermal shock strength is given by $M = 1.7_{-0.3}^{+0.5}$ (Eckert, et al. 2016).

Relic B is on the other hand a very steep spectrum relic with average spectral index of $\alpha_{relB\,235}^{610} = -1.65 \pm 0.62$. Error in spectral index is also much higher and 3σ radio emission regions of two frequencies are sometimes non co-spatial (see Fig. 3). Injection spectral index $\alpha_{inj\,235}^{610} = \alpha_{relB\,235}^{610} - 0.5$ at the front of the relic B corresponds to a Mach number of about $M = 2.02 \pm_{0.41}^{0.17}$. Where corresponding value reported by (Pearce et al. 2017) is $M = 1.86 \pm_{0.17}^{0.29}$.
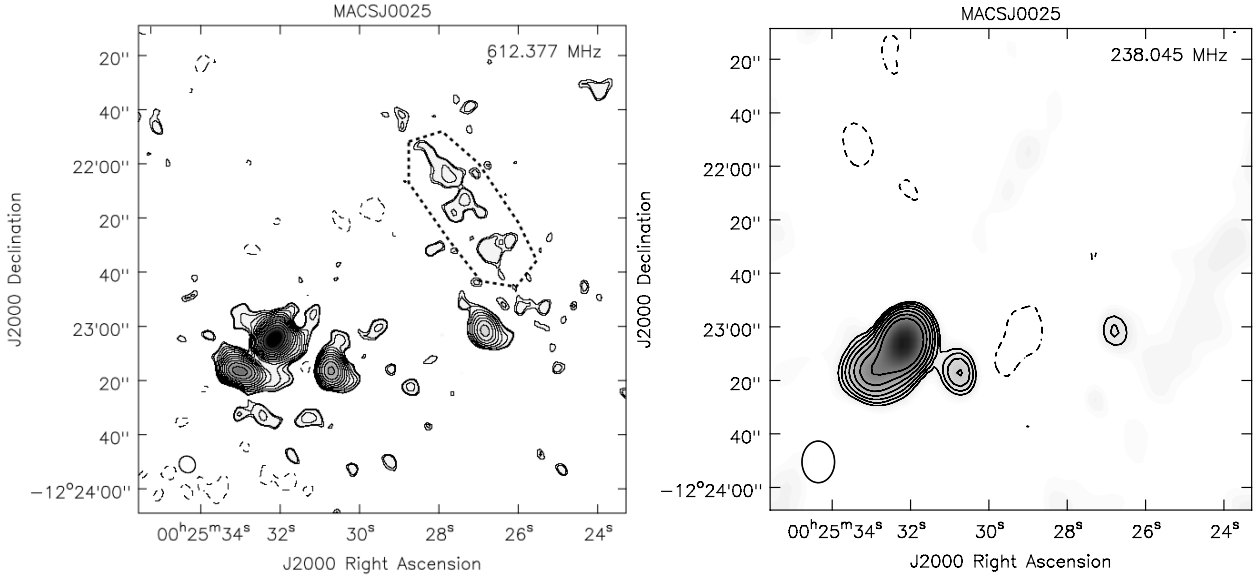
3.2 MACSJ0025.4-1222

The Cluster MACSJ0025.4-1222 is a distant cluster with redshift of z=0.584. This is a very hot and massive object with average temperature of 7.10 ± 0.70 keV. Temperature is computed from the Chandra X-ray data (Ebeling et al. 2007). It has been reported from weak and strong lensing studies that two dark matter sub-groups with similar masses (about $2.5 \times 10^{14} M_\odot$) are separated from baryonic over-density regions indicate a merger (Bradač et al. 2008) or most probably a core oscillation phase (Ma et al. 2010). High X-ray brightness of 8.8×10^{44} erg s^{-1} with presence of substructures also indicate dynamical activity in this cluster.

Evidence of diffuse radio emission, in particular relics in this cluster, was first reported by Riseley et al. (2017) at 325 MHz using the GMRT. Our GMRT observation at 610 MHz has also revealed a very faint, relic like structure towards North-West (NW) of the cluster (in RA-DEC plane) as shown in the Figure 5, Panel 1, marked with dashed line. The same structure cannot be seen in our 235 MHz map which has much higher rms caused by the data loss due to bandpass filter and presence of few bright sources in the central field. The final rms achieved is just 700 μJy beam^{-1} at 235 MHz, as compared to a much lower i.e., 90 μJy beam^{-1} at 610 MHz using the data analysis parameters mentioned in Table 2. The relic source is an extremely faint object at 610 MHz with flux density of 1.98 ± 0.30 mJy. Our re-analysed image at 325 MHz has also shown a relic like structure in the same region as in 610 MHz map, but larger in size. The observed flux density is 5.08 ± 0.75 mJy. Average spectral index measured within a common region of the relic emission from 610 and 325 MHz shows a flat spectrum of $\alpha_{325}^{610} = -1.03 \pm 0.41$. Taking the same spectrum for 610 and 325 MHz to 1.4 GHz, the $P_{1.4}$ radio power would measure to $1.19 \pm 0.18 \times 10^{24}$ WHz^{-1} and $1.60 \pm 0.24 \times 10^{24}$ WHz^{-1} respectively. But, assuming the well-known average spectral index $\alpha_{610}^{1400} = -1.3$ (Feretti et al. 2012),Riseley et al. (2017) has reported(i.e. $P_{1.4} = 1.29 \pm 0.14 \times 10^{24}$ WHz^{-1}. Apart from this relic, only 4 bright galaxies associated with some diffuse emission can be found in both the frequencies, no radio halo or any other prominent relic or diffuse emission has been detected in our maps.

We have drawn the radio contours on the Chandra archival X-ray map in Figure 6. It can be noticed that the diffuse radio emission detected at 610 and 325 MHz in this
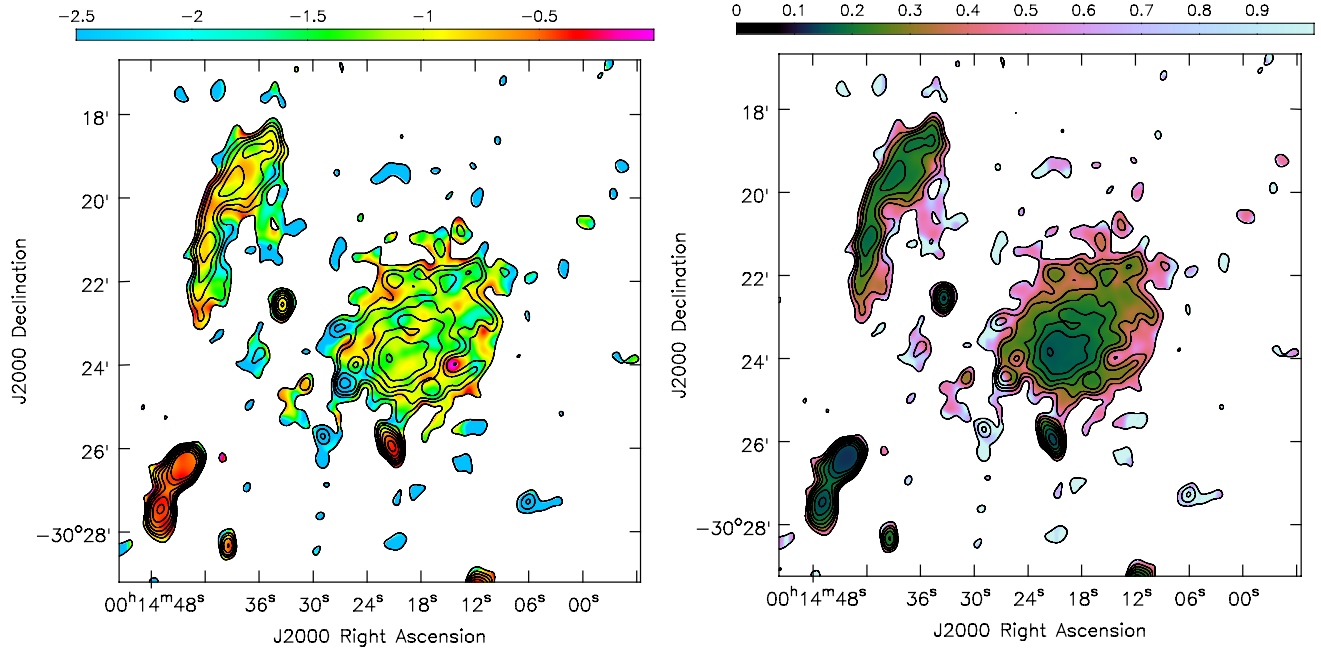
Figure 4. Panel 1: Spectral index (see Eq. 4) map of Abell 2744 in colour scale. **Panel 2:** Spectral index error (see Eq. 5) map with colour scale. Radio flux contours in both panel are same as Fig. 1.


Figure 5. Panel 1: & **Panel 2:** 610 and 235 MHz map for the cluster MACSJ0025.4-1222 with first contour at 2.5σ, rest of the contours and colour scale are same as Figure 1. The rms values at 610 MHz is $\sigma = 90\mu$Jy beam^{-1} and at 235 MHz it is $\sigma = 700\mu$Jy beam^{-1} with beam sizes as given in Table 3.

study falls at the outskirts of the X-ray core but well inside the actual extent of the cluster ($r_{500} = 1.15$ Mpc). The distance between the relic and the cluster centre is measured to be 45″ i.e., 300 kpc only. The detected relic is just 53″ in angular size which at this high redshift of z=0.584 would translate to a linear size of 350 kpc. In the re-analysed 325 MHz map, the relic measures as 68″. While, Riseley et al. (2017) have reported a size of 100″ for the same.

3.2.1 Estimated radio halo upper-limit

The expected radio power ($P^{exptd}_{1.4GHz}$) for this high mass cluster, calculated using equation 1 is $5.3 \times 10^{24} WHz$ and radio halo size, calculated using equation 2 is 1170 kpc. We have used the average slope and intercept from the Eq. 1 and Eq. 2 for the above estimations. Following the procedure given in section 2.4, using these estimated parameters, first a mock radio halo was introduced a little away from the X-ray centre of the cluster. This is done mainly
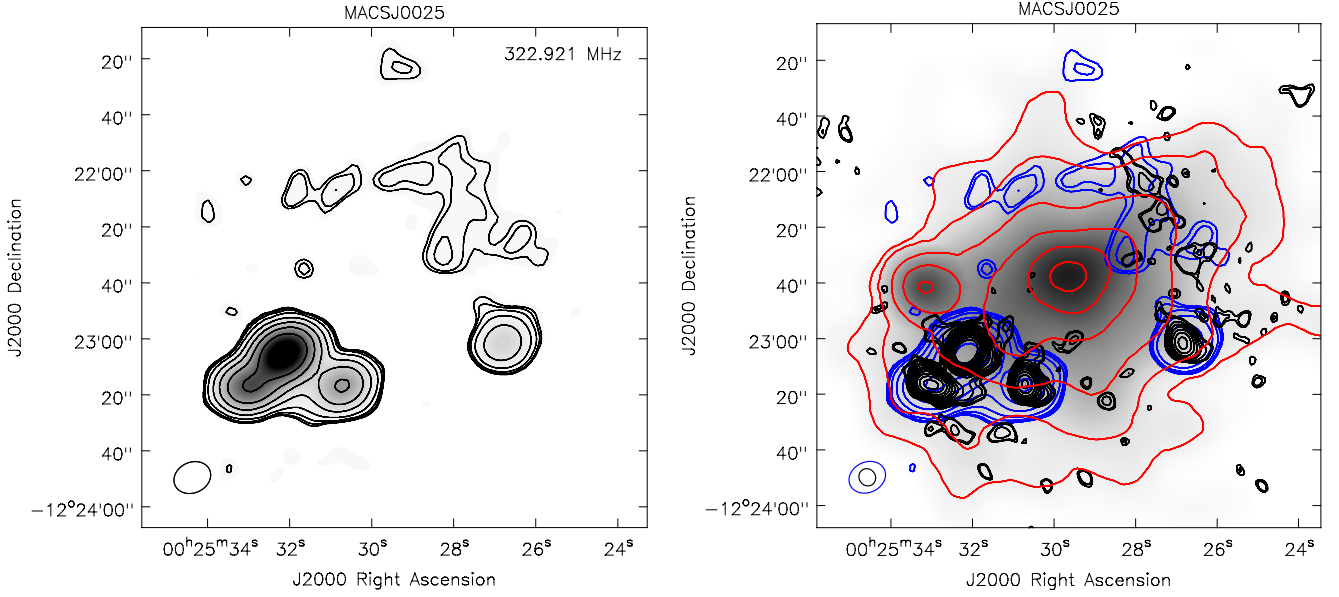
Figure 6. Panel 1: 235 MHz map for the cluster MACSJ0025.4-1222 with colour scale and controus at 3, 3.5, 4, 6, 12, 24, 48, 96 times the 1σ rms. The rms values at 325 MHz is $\sigma = 200\mu$Jy beam^{-1}. **Panel 2:** Chandra X-ray photon count (0.5-7.0 keV, Gaussian smoothed) map has been plotted in gray scale and red contours are over-plotted in red colour with contours at 1.3, 2, 4, 6, 8 and 9.5 times 2.87×10^{-8} photons s^{-1} cm^{-2} pixel^{-1}. Radio contours are in blue and black and are same as the Panel 1 of Figure 6&5 respectively.

to avoid the side-lobe interference due to the presence of central bright radio sources. The calculations were done for an image at 610 MHz, and values are then converted back to 1.4 GHz scales for reporting here. The final estimated upper limit of radio halo power ($P^{inj}_{1.4GHz}$) corresponding to injected mock halo is $4.8 \times 10^{24} WHz$. Image with the same resolution as in Figure 5 is made using the same imaging parameters. The corresponding measured power for flux above 2σ is $3.57 \times 10^{24} WHz$ and size of the recovered halo above 2σ is 582 kpc, both of which meets the criteria for halo upper limit as mentioned in Section 2.4.
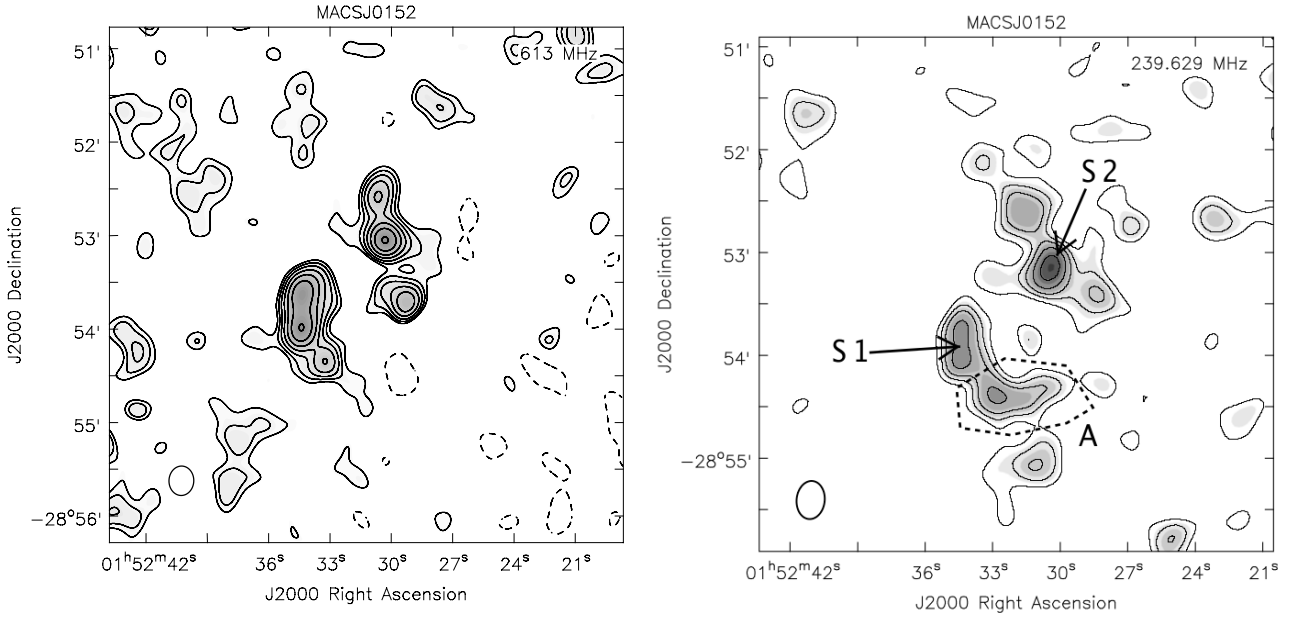
3.3 MACSJ0152.5-2852

MACSJ0152.5-2852 is another high redshift cluster at z=0.413 and moderate temperature of 4.7±0.5 keV. Its radius, r_{500} is 1.21±0.11 Mpc and mass at r_{500} is 7.9±2.2 10^{14} $M_\odot$. The cluster shows non-concentric X-ray contours towards the NW direction with the signature of substructures or disturbed morphology indicating a probable merger (Ebeling et al. 2010).

Our GMRT observation at 235 MHz has revealed a diffuse emission of about 0.5 Mpc size in this cluster. A one-sided arc-shaped radio emission is placed on the southern side of the cluster starting near to the centre to the half-way to the virial radius, marked as dashed area A in Figure 7, Panel 1. The source could not be recovered fully in 610 MHz. Except few unrelated small regions of radio emission at 235 MHz, no other prominent peripheral or arc/bow shaped relic or halo emission has been observed at both the frequencies. Among many of the radio sources, only two radio bright spots marked as S1 and S2 in Figure 7 Panel 2 are of point source origin. One is connecting to the left arc-like radio structure, marked as S1 and other on the right side marked

as S2. These two sources can be correlated with the optical and bright X-ray counterparts (See Fig. 8, both panels), and they are the radio and X-ray bright galaxies. Coincidentally, these two bright sources are placed at the centre of the two galaxy groups (X-ray sources: Ebeling et al. 2010) that are supposed to be colliding with each other. Rest part of the left radio structure i.e., other than S1, has no optical and X-ray counterparts of compact point source origin and are purely diffuse in nature (see Fig. 8, both panels). The total flux density of this arc-like structure at 235 MHz is 9.24 ± 1.30 mJy (radio power of $5.68 \pm 0.80 \times 10^{24}$ W Hz^{-1}) and spectral index of the part of the source that has been observed in both 610 and 235 MHz is extremely steep $\alpha_{rel} = -2.3 \pm 0.58$. Size of this diffuse radio structure is about $1.5'$, though at high red-shift that translate to about 0.5 Mpc.

3.3.1 Estimated radio halo upper-limit

Adopting average slopes and intercept given in Eq. 1 and Eq. 2, the computed possible radio halo power ($P^{exptd}_{1.4GHz}$) for cluster MACSJ0152.5-2852 is $4.13 \times 10^{24} WHz$ and expected radio halo size is 1108 kpc. Radio halo upper limit is thereafter evaluated performing the steps mentioned in Section 2.4. Calculations were done for an image at 610 MHz and scaled 1.4 GHz values are reported here. The final estimated value of upper limits of halo power ($P^{inj}_{1.4GHz}$) is $3.29 \times 10^{24} WHz$. Image with the same resolution as in Figure 7 is made using the same procedure. The radio power corresponding to measured flux above 2σ is $1.53 \times 10^{24} WHz$ and size of recovered halo measured above 2σ is 588 kpc which corresponds well with our criteria mentioned in section 2.4 for calculating halo upper limits.

Figure 7. Panel 1: & **Panel 2:** Same as Figure 1 for the cluster MACSJ0152.5-2852. Only the rms values at 610 MHz is $\sigma = 70\mu$Jy beam^{-1} and at 235 MHz it is $\sigma = 500\mu$Jy beam^{-1}. S1 and S2 are the two point sources having optical and X-ray counter part. Dashed line encloses the extended diffuse relic (?).
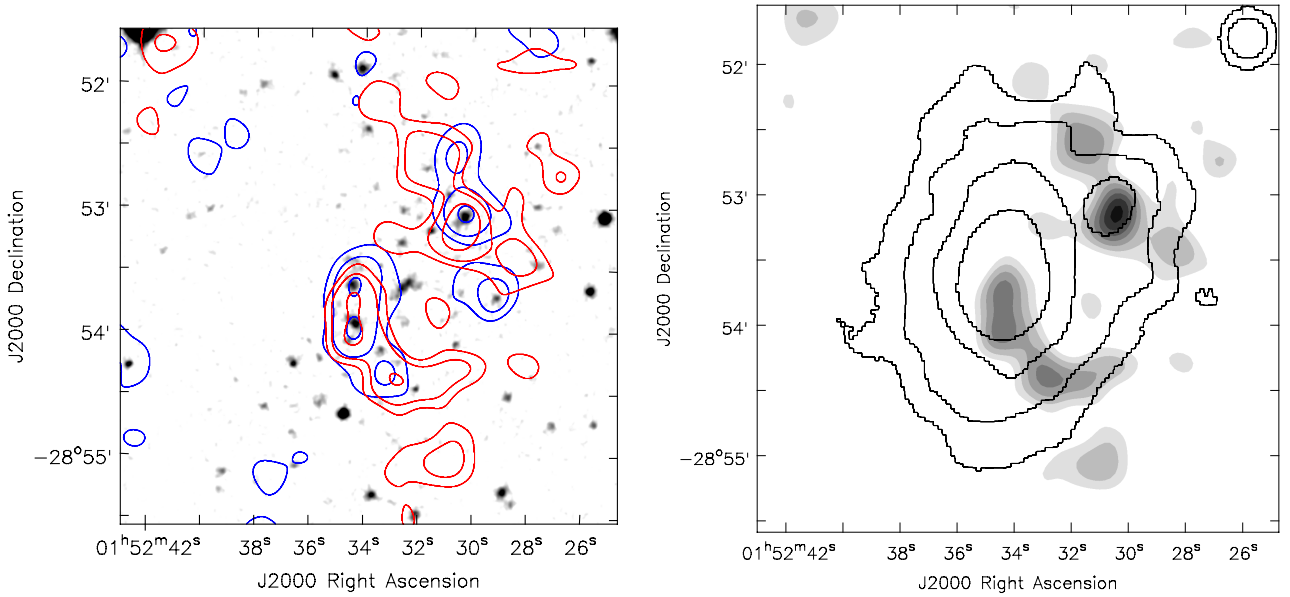

Figure 8. Panel 1: GMRT 610 (blue) and 235 MHz (red) contours (only 3 at 3,6,12 $\sigma = 70\&500\mu$Jy beam^{-1}) are over plotted on SDSS optical image. **Panel 2:** Chandra X-ray photon count map (0.5-7.0 keV, Gaussian smoothed) with black contrours at 4,8,16 and 32 times 10^{-8} photons s^{-1} cm^{-2} pixel^{-1} and are over plotted on the gray colour radio map of MACSJ0152.5-2852 at GMRT 235 MHz.

3.4 MACSJ1931-2635

The clusters MACSJ1931-2635 did not show any clear diffuse radio emission at both the frequencies (See Fig. 9, both panels). This cluster only shows an interesting radio galaxy with extremely bent jets with jet separation angle of about 30° as seen at 610 MHz. But, jets could not be resolved in 235 MHz map. Our low resolution maps in Figure 9 have rms of 1200 and 80μJy beam^{-1} respectively at 235 and 610 MHz for beam sizes of $17.37'' \times 11.93''$ and $7.55'' \times 5.22''$. Be-cause of presence of a bright central radio source in this cluster, produced image is dynamic-range limited. Therefore, no interesting diffuse radio emission could be detected. Further, Chandra X-ray photon counts map shows comparatively smooth gas distribution. X-ray emission is mostly dominated by the central galaxy perfectly coinciding with radio galaxy core.
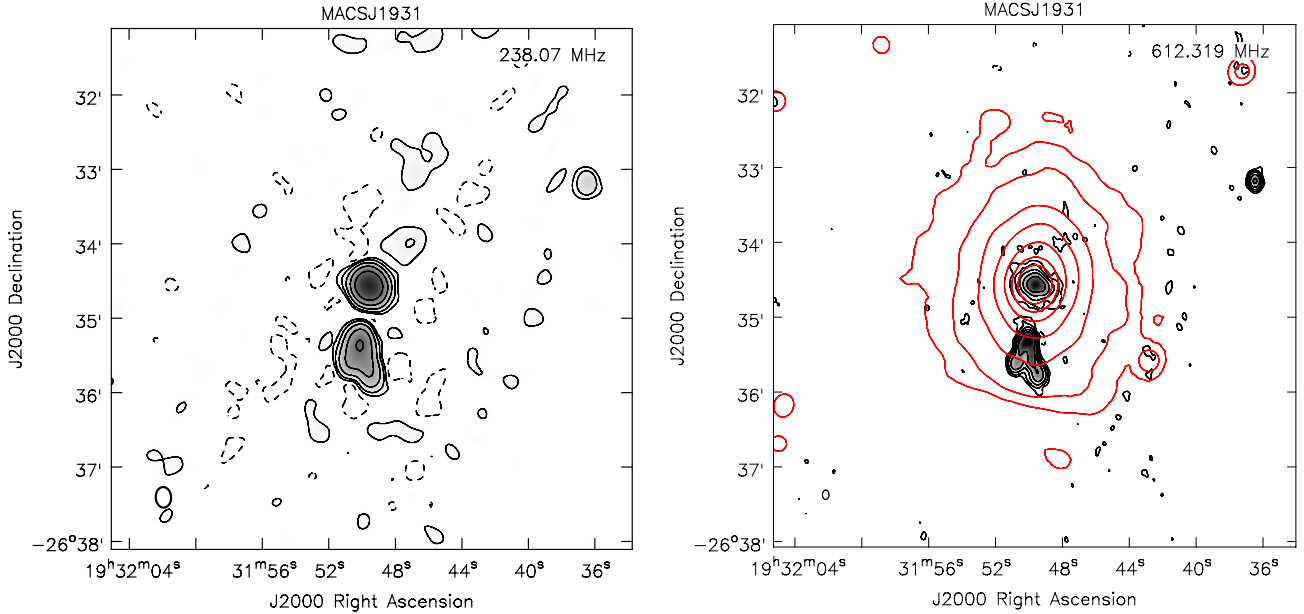
Figure 9. Panel 1: GMRT 235 MHz map of the cluster MACSJ1931-2635 plotted in gray. Black contours are radio fluxes at the level of 3σ (where rms i.e. $\sigma = 1200\mu$Jy beam^{-1}) and rest of the conours are at 9,27,81,243 σ. We have also plotted a -3σ contour with black dashed line. **Panel 2:** Same contours as Panel 1 at 610 MHz with rms $\sigma = 80\mu$Jy beam^{-1}. Red controus are the Chandra X-ray photon count map of 0.5-7.0 keV (Gaussian smoothed).

4   DISCUSSIONS

4.1   Cluster with a unique radio halo-relic structure

We report the low frequency radio spectral and morphological signatures of Abell 2744, a rare radio halo-relic system through high resolution and deep radio images from GMRT dual band (610 & 235 MHz) observations. Systems with the prominent peripheral bow shaped relic/s are usually devoid of central halos and only a few of the clusters are known to host both halo and relic (Giovannini & Feretti 2004). This makes Abell 2744 cluster a very rare one. The dimension (LLS) of the relic and the halo in this cluster is observed to be one of the largest, as both of them are about 1.6 Mpc in size at 235 and 610 MHz as seen in this study (at 3σ level respectively; see Section 3.1.1 and 3.1.2). Orrú et al. (2007) has reported a similar size (both ~ 1.6 Mpc) as ours at 325 MHz VLA. At GMRT 325 MHz the sizes measured from our re-analysed image are further bigger, 1.85 and 1.82 Mpc respectively. The sizes reported so far at various observing frequencies (200 MHz - 4 GHz) vary from 1.0-2.34 Mpc for the halo and 1.1 - 2.0 Mpc for the relic A as shown in the Table 5. So far, the known halos bigger than this are 3.1 Mpc in CIZAJ2242.8+5301, 2.9 Mpc in Abell 2163 (van Weeren et al. 2010; Hoang, et al., 2017; Feretti et al. 2001) and bigger relic is 2.5 Mpc in Abell 115 Govoni et al. 2001b). Additionally, this cluster hosts a second relic (i.e. Relic B) that was first reported by Pearce et al. (2017) at high frequency, and we confirm it at low frequencies. Relic B has a size of over a Mpc at 1-4 GHz which we report as 0.9-1 Mpc at 235, 610 MHz and at 325 MHz the size is ~ 0.7 Mpc as found in our study as well as reported in Venturi et al. (2013) as a radio bridge.

Average spectral index of both relic A and the halo in

Table 5. Multi-frequency radio structures of Abell 2744

Frequencies	LLS (Mpc)		
(MHz)	(Halo:	Relic A:	Relic B:)
200 (GLEAM)[a]	1.01	1.10	–
235 (GMRT)[b]	1.55	1.49	0.98
325 (VLA)[c]	1.6	1.6	–
325 (GMRT)[d]	1.9	1.3	–
325 (GMRT)[b]	1.85	1.82	0.74
610 (GMRT)[b]	1.59	1.49	0.86
1400 (VLA)[e]	2.34	2.0	–
1500 (VLA)[f]	~ 2.1	~ 1.5	~ 1.15
3000 (VLA)[f]	~ 2.1	~ 1.5	~ 1.15

(a) George et al. (2017) **(b)** Current study **(c)** Orrú et al. (2007)
(d) Venturi et al. (2013) **(e)** Govoni et al. (2001b)
(f) Pearce et al. (2017)

this cluster is strikingly similar i.e., ($\alpha_{relA}{}^{235}_{610} = -1.14 \pm 0.36$ and $\alpha_{halo}{}^{235}_{610} = -1.17 \pm 0.33$; see Section 3.1.3). Average spectral index in wide, low-frequency range i.e., between 235, 325 and 610 MHz has also been computed and found to be $\alpha_{relA}235, 325\&610 = -1.09 \pm 0.20$ and $\alpha_{halo}235, 325\&610 = -1.21 \pm 0.20$. Venturi et al. (2013) have reported spectral index between 325 and 1400 MHz as $\alpha_{relA}{}^{325}_{1400} = -1.24 \pm 0.10$, and $\alpha_{halo}{}^{325}_{1400} = -1.19 \pm 0.08$ and for the high frequency range i.e., 1.5 to 3 GHz it is $\alpha_{relA}{}^{1500}_{3000} = -1.32 \pm 0.09$ and $\alpha_{halo}{}^{1500}_{3000} = -1.43 \pm 0.11$ (see Tab. 6). Interestingly though, at low frequency the spectral index is flatter and at high frequency it is reported to be little steeper, at respective frequency ranges, both halo and relic has comparable spectral index.

Table 6. Multi-band radio spectrum of Abell 2744

Frequencies (MHz)	Spectral Index		
	(Halo:	Relic-A:	Relic-B:)
118,154,200, $\Big\}$ [a] 325 & 1400	-1.09 ± 0.05	-1.01 ± 0.07	–
325 & 1400[b]	-1.0 ± 0.1	-1.1 ± 0.1	–
325 & 1400[c]	$-1.19^{+0.08}_{-0.11}$	-1.24 ± 0.10	–
235 & 610[e]	-1.17 ± 0.33	-1.14 ± 0.36	-1.65 ± 0.62
235,325 & 610 [e]	-1.21 ± 0.20	-1.09 ± 0.20	-1.34 ± 0.16
235 & 1400[e]	-1.20 ± 0.12	-1.25 ± 0.15	–
1500 & 3000[d]	-1.43 ± 0.11	-1.32 ± 0.09	-1.81 ± 0.26

(a) George et al. (2017); (GLEAM-TGSS-VLA)
(b) Orrú et al. (2007); (VLA-VLA)
(c) Venturi et al. (2013); (GMRT-VLA)
(d) Pearce et al. (2017) ; (VLA-VLA)
(e) Current study; (GMRT-GMRT)

4.2 Understanding halo-relic co-existence

Observations show that relic A in this cluster is a one-sided (with no counterpart), peripheral, curved-relic with its concave side facing the central halo and matching the halo curvature as observed in Fig. 3. This indicates that the shocks must be spheroidally evolving after cluster mergers as noticed in Paul et al. (2011). Unlike the usual peripheral relics, which form almost along the merging axis (Bagchi et al. 2006), relic A has formed towards the perpendicular direction to the observed axis of current substructure merger (see Section 3.1.2). Apart from this, the other significant finding from this study is a proposed high Mach number ($M = 2.02^{+0.17}_{-0.41}$) internal shock (see Section 3.1.3) which we have reported above as relic B.

Figure 1 shows that the prominent relic A in this cluster is about 1.7 Mpc away from the centre, an average speed of 1,000 km/s for the shock (Sarazin 2002) would mean that the merger had taken place at about 1.7 Gyr ago. But, electrons lose energy very fast through synchrotron emission (Boozer 2015). Unless, a continuous and in situ particle acceleration engine is present in cluster, synchrotron emission remains visible only about a few hundred Mega years (i.e., equivalent to Synchrotron and IC cooling time; Kang et al. 2017; Kang 2016). Usually, relics are always attached to the shocks that are acting as in situ particle accelerators, and eventually survive for long (~ 2 Gyr), till the shock is powerful enough to energise ambient electrons to relativistic energy. But, turbulence in the cluster centre is found to be effective enough to produce radio emission for only about one Gyr after each merger (Cassano et al. 2016; Cassano & Brunetti 2004). Therefore, if the turbulent re-acceleration (TRA) is considered to be the only mechanism responsible for radio halo emission, a cluster that has merged more than a Gyr ago may not keep its radio halo alive. Even if, it remains alive it cannot be observed in high frequencies, as spectrum would be extremely steep (Brunetti et al. 2001). Which is not the case for cluster Abell 2744, having a flat spectrum, bright halo even at 4 GHz (Pearce et al. 2017). This indicates either a different particle acceleration scenario or a recent activity that would re-accelerate the ambient electrons to reproduce the halo. If, the first merger is not an immediate event, a flat spectrum halo would indicate a second possible

event that has recently re-accelerated the ambient electrons (Markevitch et al. 2005). So, presence of the second closer relic (Relic B) may help to resolve this issue.

The second relic in Abell 2744 i.e., Relic B has been found well within one Mpc from the centre and possibly connected to the merging sub-cluster (the brightest point inside the observed halo) that is seen to move towards SE direction. Its distance is only about < 0.7 Mpc from this sub-clump. This shock has Mach number of about $M = 2.02 \pm^{17}_{41}$ as computed from its injection spectral index of $\alpha_{inj} = 1.15$ (see Sec. 3.1.3). This gives a shock speed of about $1769 \pm^{148}_{359}$ km/s in a medium with temperature of about 3.5×10^7 K (as seen in Pearce et al. 2017). The shock velocity (V_{sh}) has been computed from the relation $V_{sh} = M 1480 T_g 10^8 K^{12} km\,s^{-1}$ (Sarazin 1988) where T_g is the temperature of the ICM gas. Further, this would mean that the shock has passed through the cluster halo within last $387 \pm^{98}_{30}$ Myrs, indicating a very recent second merger. In fact, a similar two merger scenario has been proposed by Medezinski, et al. (2016), as concluded from their weak lensing study. They propose that, the first i.e., the major merger event had taken place along the East-West direction and a newer merger along the North-South direction. Eventually, this may provide a possible explanation for the observed, long-lasting, flat spectrum radio halo in connection to turbulent re-acceleration process, though does not rule out the possibility of any other scenario.

4.3 Possible evidence of early stage mergers?

4.3.1 MACSJ0025.4-1222

Here, we report the detection of a very faint (Flux density of 1.98 ± 0.30 mJy) radio relic like structure in the NW side of the cluster MACSJ0025.4-1222 at GMRT 610 MHz. Also, it has been confirmed at 325 MHz map (see Fig. 6, Panel 1). Detection of cluster diffuse radio sources become difficult at so high redshift (z=0.584). Only a deeper observation may reveal the full structures. Therefore, observed diffuse radio emission from such a high redshift cluster itself a significant event. This also informs us about a galaxy cluster merger that has taken place at such an early stages (at high redshift) of structure formation in the Universe.

Fig. 6 shows that the relic in MACSJ0025.4-1222 is placed at just outside the X-ray core of the cluster (Bradač et al. 2008) i.e., about 300 kpc or $45''$ from the centre. If, the relic has originated due to a merger, it should be a recent merger, since the shock has merely travelled a 300 kpc distance. An average speed of 1000 km/s for the shock would account for a time of 300 Myr only. In such a situation, we would also expect to detect a radio halo as well. But, we have not detected any other diffuse radio emission, or found no information regard to this in literature. Non detection of a halo may be attributed to the limit of sensitivity of the particular observation, less turbulence in the medium or to a different particle acceleration mechanism. A detection or non-detection of halo with deeper observation would thus be interesting in connection to constraining possible particle acceleration mechanism and dynamical condition of the ICM. This distant cluster is thus an important object, one of the few earliest (next only to El Gordo cluster; z=0.87; Lindner et al. (2014)), and possibly the young merging systems detected in radio waves.

4.3.2 MACSJ0152.5-2852

We have discovered a faint (total flux density 9.24 ± 1.30 mJy) and extended, relic-like diffuse radio structure of size of about 0.5 Mpc in MACSJ0152.5-2852 cluster at 235 MHz.

Unlike most of the arc-shaped radio relics that are observed almost at the virial radius of the host clusters, location of this source is well inside the virial radius (see Fig. 8, Panel 2). The only bright, point like source (S1) is co-incidentally falling at the X-ray centre of the bigger galaxy group and co-positioned with a radio X-ray bright galaxy residing at the centre of the cluster. As discussed in Section 3.3, the other part of the arc like radio structure is purely of diffuse in nature and is extended to about 0.5 Mpc towards the outskirts of the cluster. Presence of a small group of galaxies in NW of the cluster, most probably falling in to the bigger group towards SE (found in X-ray map), indicates an ongoing activity i.e., a merger (Fig. 8). So, the diffuse structure detected in this cluster may be a relic that has been originated from this merger and considering its position closer to the cluster centre, must be originated within last half a Gyr. But, the spectral index of the common part of the diffuse radio structure that has been observed with both 610 and 235 MHz, is extremely steep $\alpha_{rel} = -2.3 \pm 0.58$. Such steep spectrum is also a characteristic of a radio phoenix. Therefore, further deeper map at these frequencies, as well as at lower frequency (i.e., GMRT 150 MHz), are a must to get a complete and clear picture of this cluster.

4.4 Fitting observed halos and relics into existing correlations

Radio halo power (at 1.4 GHz) of massive clusters is known to follow a steep slope correlation (BCES bisector slope 3.70 ± 0.56 and 2.11 ± 0.20) with cluster mass (M_{500}) and X-ray luminosity (L_{500}) respectively (Cassano et al. 2013). A possible correlation between the relic power (at 1.4 GHz) and its size (LLS), has also been reported by Feretti et al. (2012). So, it is useful to check, where our studied halos and relics stand with respect to these well-known correlations.

As reported in this study, only one (i.e. Abell 2744) among the four observed clusters has been detected with a radio halo. In total, three of them show relics (except MACSJ1931-2635). Since, our study was done at low frequencies, we have projected our observed radio powers to 1.4 GHz using the reported spectral index $\alpha_{235}^{1400} = -1.20, -1.25$ (see Table 6) for Abell 2744, $\alpha = -1.03$ (see Section 3.2) for cluster MACSJ0025.4-1222, and assumed $\alpha_{610235}^{1400} = -1.3$ for the rest of the sources. Our estimated radio powers are reasonably closer to the values reported in (Pearce et al. 2017) and are given as $P_{1.4} = 1.16 \pm 0.12 \times 10^{25}\ W\ Hz^{-1}$, $4.89 \pm 0.5 \times 10^{24}\ W\ Hz^{-1}$ and $4.5 \pm 0.6 \times 10^{23}\ W\ Hz^{-1}$ respectively for the same structures. For the cluster MACSJ0025.4-1222, the projected relic radio power is $P_{1.4} = 1.19 \pm 0.18 \times 10^{24}\ WHz^{-1}$ in our study which is comparable to $P_{1.4} = 1.29 \pm 0.14 \times 10^{24}\ WHz^{-1}$ reported in Riseley et al. (2017). We found the relic power in MACSJ0152.5-2852 to be $5.58 \pm 0.78 \times 10^{23}\ WHz^{-1}$. Our estimated radio halo upper limits at 1.4 GHz for the above two clusters are given by $4.8 \times 10^{24}\ W\ Hz^{-1}$ and $3.29 \times 10^{24}\ W\ Hz^{-1}$ (see Section 3.2.1 and 3.3.1).

Figure 10, Panel 1, shows the correlation M_{500} vs $P_{1.4}$

Table 7. Correlation slopes

Correlations	Old slope	New slope
Radio Halo		
M_{500} vs $P_{1.4}$	3.04 ± 0.33	2.96 ± 0.29
L_{500} vs $P_{1.4}$	1.57 ± 0.28	1.58 ± 0.28
Radio Relic		
LSS vs $P_{1.4}$	1.90 ± 0.26	1.88 ± 0.24

i.e., between the mass of clusters (within radius r_{500} i.e., M_{500}) and the radio power of the halos at 1.4 GHz (i.e., $P_{1.4}$). Figure 10, Panel 2 shows the correlation between X-ray luminosity (L_{500}) and 1.4 GHz radio power ($P_{1.4}$). Data plotted from the literature are GMRT Radio Halo Surveys (GRHS) and, some individual studies with various telescopes (Cassano et al. 2013; Bernardi et al. 2016; Giacintucci, et al. 2014). The upper limits are estimated for the undetected Extended-GRHS sources by Venturi et al. (2013). Our only detected halo has been plotted as a red point and, two upper limits are plotted as red down arrows. Figure 11 shows the plot of radio power versus size (LLS) of the relics. Here we have plotted our observed relics on the results reported in Feretti et al. (2012). We have computed the BCES bisector fitting slopes and confidence levels for already available data as well as combining with data from current study. The old and the new slopes and their corresponding errors are reported in Table 7. No considerable change of slopes can be noticed after adding new data from the current study.

5 CONCLUSIONS

We have observed four galaxy clusters selected from MACS list at GMRT low frequency (235 and 610 MHz) radio waves to study the morphology and spectral properties to understand their dynamical features as well as their candidature to the existing pool of cluster radio structures. Among the four observed clusters, three of them namely, MACSJ0014.3-3022 or Abell 2744, MACSJ0025.4-1222 and MACSJ0152.5-2852 are detected with diffuse radio emission. But, cluster MACSJ1931.8-2635 did not show any diffuse emission at the rms noise level (local) of 80 and 1200 μJy beam^{-1} at 610 and 235 MHz respectively in our observations.

• The deep low-frequency radio maps show both a giant halo and multiple relics in the cluster MACSJ0014.3-3022 i.e., Abell 2744, possibly the largest halo relic combination at both low and high frequency radio waves (1.6 Mpc each in this study and at maximum 2.4 and 2 Mpc respectively from literature). The almost spherical, text book type, halo observed in Abell 2744 indicated to have a different origin than the merging event responsible for producing relic A, which is estimated to have originated more than 1.5 Gyr ago. Here, we also confirm the detection of a second relic i.e., relic B (at low frequencies i.e., 235 and 610 MHz), very near (< 0.7 Mpc) to the cluster core. The relic has possibly originated from a high Mach number ($\mathcal{M} = 2.02$) shock with a computed shock speed of $1769 \pm_{359}^{148}$ km/s due to a second and ongoing merger along NW to SE direction as
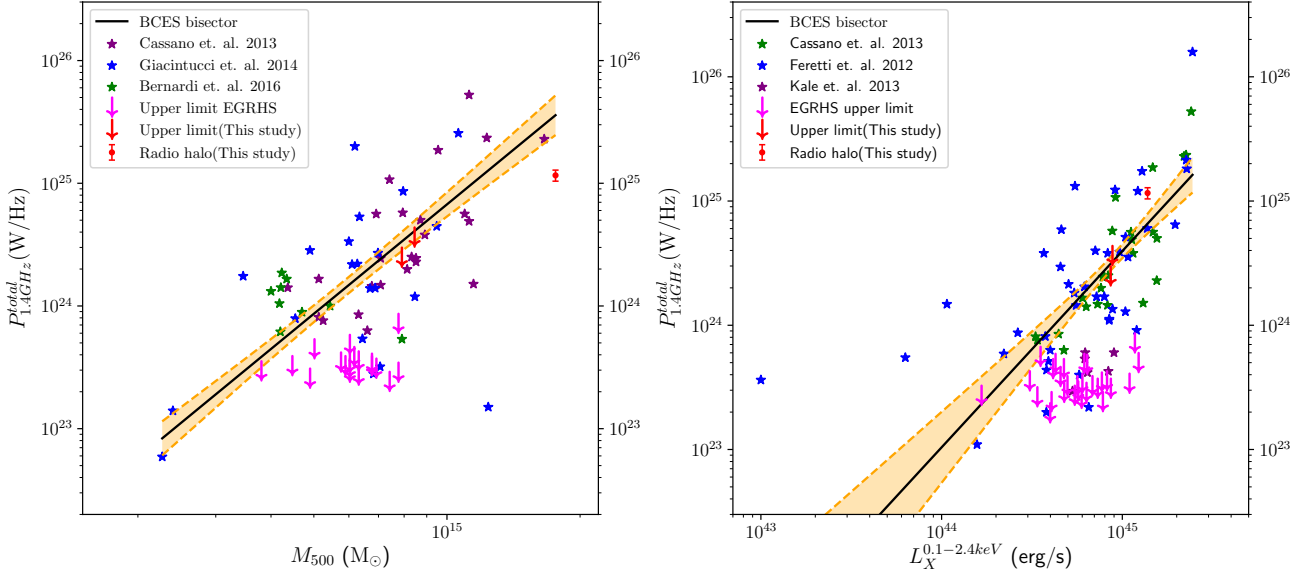
Figure 10. Plotted radio power ($P_{1.4GHz}$) against virial mass (M_{500}, Panel 1) and X-ray luminosity (L_{500}, Panel 2). Data points are taken from various studies as mentioned in legends. Data and upper limits from current study is plotted in red colour. BCES Bisector fitting slope (black line) and confidence levels are drawn at 95% (orange) i.e. about 2σ (see Table 7).
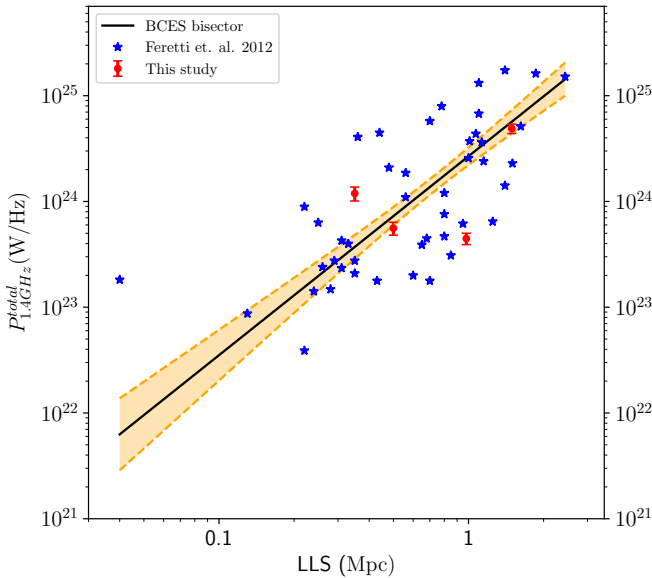
Figure 11. Plotted radio power ($P_{1.4GHz}$) against Largest Linear Size (LLS) of the relics. Colour code is as mentioned in the legend. Fitting details are same as Fig. 10.

understood from the current study and earlier weak lensing study. Lastly, a marginal but same amount of ageing effect reported in this study for both halo and the relic needs to be investigated further.

• We report here the detection of radio relic-like diffuse emission in two of our galaxy clusters MACSJ0152.5-2852 and MACSJ0025.4-1222. These 2200 Mpc and 3500 Mpc (luminosity distance and $z = 0.413$ & 0.584 respectively) away clusters observed to host diffuse radio structures of sizes $\lesssim$ 0.5 Mpc well inside their virial radius. Both these clusters being at high redshift are possible evidence of early universe and early stage merging systems.

• All detected halo and relic reported in this study shown to fit well with the prevailing radio power vs mass, X-ray luminosity as well as LLS correlations and therefore they are a good addition to the existing data set of radio halos and relics.

• We also report the non-detection of diffuse radio emission from galaxy cluster MACSJ1931-2635.

REFERENCES

Bagchi, J., Durret, F., Neto, G. B. L., & Paul, S. 2006, *Science*, 314, 791

Blandford, R., & Eichler, D. 1987, *Physics Report*, 154, 1

Bernardi, G., Venturi, T., Cassano, R., et al. 2016, MNRAS, 456, 1259

Bonafede, A., Brüggen, M., van Weeren, R., et al. 2012,*MNRAS*, 426, 40

Bonafede, A., Cassano, R., Brüggen, M., et al. 2017, MNRAS, 470, 3465

Boozer, A. H. 2015, Physics of Plasmas, 22, 032504

Borgani, S., & Guzzo, L. 2001, Nature, 409, 39

Bradač, M., Allen, S. W., Treu, T., et al. 2008, ApJ, 687, 959

Brown, S., Duesterhoeft, J., & Rudnick, L. 2011, ApJ, 727, L25

Brunetti, G., Setti, G., Feretti, L., & Giovannini, G. 2001, MN-RAS, 320, 365

Bykov, A. M., Dolag, K. and Durret, F., 2008, *SSRv.*, 134, 119

Cassano, R., & Brunetti, G. 2004, Journal of Korean Astronomical Society, 37, 583

Cassano, R., Brunetti, G., Setti, G., Govoni, F., & Dolag, K. 2007, MNRAS, 378, 1565

Cassano, R., Ettori, S., Giacintucci, S., et al. 2010, ApJ, 721, L82

Cassano, R., Brunetti, G., & Venturi, T. 2011, *Journal of Astrophysics and Astronomy*, 32, 519

Cassano, R., Ettori, S., Brunetti, G., et al. 2013, ApJ, 777, 141

Cassano, R., Brunetti, G., Giocoli, C., & Ettori, S. 2016, A&A, 593, A81

Colafrancesco, S., Marchegiani, P., & Paulo, C. M. 2017, MNRAS, 471, 4747

Donnert, J., Dolag, K., Brunetti, G., & Cassano, R. 2013, MN-RAS, 429, 3564

Ebeling H., Edge A. C. and Henry J. P., 2001, *ApJ*, 553, 668

Ebeling, H., Barrett, E., Donovan, D., et al. 2007, ApJ, 661, L33

Ebeling, H., Edge, A. C., Mantz, A., et al. 2010, *MNRAS*, 407, 83

Eckert, D., Jauzac, M., Vazza, F., et al. 2016, MNRAS, 461, 1302.

Ensslin, T. A., Biermann, P. L., Klein, U., & Kohle, S. 1998, A&A, 332, 395

Feretti, L., Fusco-Femiano, R., Giovannini, G., & Govoni, F. 2001, A&A, 373, 106

Feretti, L., & Giovannini, G. 2008, A Pan-Chromatic View of Clusters of Galaxies and the Large-Scale Structure, 740, 24

Feretti, L., Giovannini, G., Govoni, F., & Murgia, M. 2012, A&ARv, 20, 54

George, L. T., Dwarakanath, K. S., Johnston-Hollitt, M., et al. 2017, MNRAS, 467, 936

Giacintucci, S., Markevitch, M., Venturi, T., et al. 2014, ApJ, 781, 9.

Giovannini, G., Tordi, M., & Feretti, L. 1999, *New Astronomy*, 4, 141

Giovannini G., & Feretti, L. 2004, *JKAS*, 37, 323

Giovannini, G., Bonafede, A., Feretti, L., et al. 2009, A&A, 507, 1257

Govoni, F., Enßlin, T. A., Feretti, L., & Giovannini, G. 2001, A&A, 369, 441

Govoni, F., Feretti, L., Giovannini, G., et al. 2001, A&A, 376, 803

Hoang D. N., et al., 2017, *MNRAS*, 471, 1107

Hoeft, M., Brüggen, M., 2007, *MNRAS*, 375, 77

Horesh A., Maoz D., Ebeling H., Seidel G., and Bartelmann M., 2010, *MNRAS*, 406, 1318

Iapichino L., & Brüggen M. 2012, *MNRAS*, 423, 2781

Intema, H. T., Jagannathan, P., Mooley, K. P., & Frail, D. A. 2017, A&A, 598, A78

Johnston-Hollitt, M., & Pratley, L. 2017, arXiv:1706.04930

Kale, R., Dwarakanath, K. S., Vir Lal, D., et al. 2016, Journal of Astrophysics and Astronomy, 37, 31

Kang, H. 2016, Journal of Korean Astronomical Society, 49, 83

Kang, H., Ryu, D., & Jones, T. W. 2017, ApJ, 840, 42

Kempner, J. C., & David, L. P. 2004, MNRAS, 349, 385

Kim, J.-Y., & Trippe, S. 2014, Journal of Korean Astronomical Society, 47, 195

Lindner, R. R., Baker, A. J., Hughes, J. P., et al. 2014, ApJ, 786, 49

Ma, C.-J., Ebeling, H., Marshall, P., & Schrabback, T. 2010, MN-RAS, 406, 121

Mahler, G., Richard, J., Clément, B., et al. 2018, MNRAS, 473, 663

Mantz, A., Allen, S. W., Ebeling, H., Rapetti, D., & Drlica-Wagner, A. 2010, MNRAS, 406, 1773

Markevitch M., Govoni F., Brunetti G., & Jerius D. 2005, *ApJ*, 627, 733

McMullin, J. P., Waters, B., Schiebel, D., Young, W., & Golap, K. 2007, Astronomical Data Analysis Software and Systems XVI, 376, 127

Murgia, M., Govoni, F., Markevitch, M., et al. 2009, A&A, 499, 679

Medezinski, E., Umetsu, K., Okabe, N., et al. 2016, ApJ, 817, 24.

Nuza, S. E. and Hoeft, M. and van Weeren, R. J. and Gottlöber, S. and Yepes, G., 2012, *MNRAS*, 420, 2006

Nuza, S. E., Gelszinnis, J., Hoeft, M., & Yepes, G. 2017, MNRAS, 470, 240

Orrú, E., Murgia, M., Feretti, L., et al. 2007, A&A, 467, 943

Rephaeli, Y., Nevalainen, J., Ohashi, T., & Bykov, A. M. 2008, *SSRv*, 134, 71

Riseley, C. J., Scaife, A. M. M., Wise, M. W., & Clarke, A. O. 2017, A&A, 597, A96

Rottgering, Wieringa, H. J. A., Hunstead, M. H., R. W., & Ekers, R. D. 1997, *MNRAS*, 290, 577

Paul, S., Datta, A., & Intema, H. T. 2014, Astronomical Society of India Conference Series, 13, 187

Paul, S., Datta, A., Malu, S., et al. 2018A, arXiv:1804.02588

Paul, S., Gupta, P., John, R. S., & Pubjabi, V. 2018, arXiv:1803.10764

Pearce, C. J. J., van Weeren, R. J., Andrade-Santos, F., et al. 2017, ApJ, 845, 81

Pinzke, A., Oh, S. P., & Pfrommer, C. 2017, MNRAS, 465, 4800

Sarazin, Craig L., 1986, *Rev. Mod. Phys.*, 58, 1

Sarazin, C. L. 1988, Cambridge Astrophysics Series, Cambridge: Cambridge University Press, 1988,

Sarazin, C. L. 2002, Merging Processes in Galaxy Clusters, 272, 1

Skillman, S. W., Hallman, E. J., O'Shea, B. W., et al. 2011, *ApJ*, 735, 96

S. Paul, L. Iapichino, F. Miniati, J. Bagchi & K. Mannheim 2011, *ApJ*, 726, 17

S. Paul, 2012, *Journal of Physics: Conference Series*, 405, 012026

Stroe, A., van Weeren, R. J., Intema, H. T., et al. 2013, A&A, 555, A110

Stroe, A., Rumsey, C., Harwood, J. J., et al. 2014, MNRAS, 441, L41.

Subramanian, K., Shukurov, A., & Haugen, N. E. L. 2006, *MNRAS*, 366, 1437

van Weeren, R. J., Röttgering, H. J. A., Bagchi, J., et al. 2009, *A&A*, 506, 1083

van Weeren, R. J., Röttgering, H. J. A., Brüggen, M., & Hoeft, M. 2010, Science, 330, 347

van Weeren, R. J., Röttgering, H. J. A., Intema, H. T., et al. 2012, A&A, 546, A124

Venturi, T., Giacintucci, S., Dallacasa, D., et al. 2008, A&A, 484, 327

Venturi T., Giacintucci S., Dallacasa D., et al. 2013, A&A, 551, A24

Zitrin A., Broadhurst T., Barkana R., Rephaeli Y., and Benítez N., 2011, *MNRAS*, 410, 1939